CMS Physics Analysis Summary

Contact: cms-pag-conveners-susy@cern.ch 2017/03/28

Search for new physics in final states with two opposite-sign, same-flavor leptons, jets, and missing transverse momentum in pp collisions at $\sqrt{s} = 13$ TeV

The CMS Collaboration

Abstract

A search is presented for physics beyond the standard model in final states with two opposite-sign, same-flavor leptons, jets, and missing transverse momentum. The data sample corresponds to an integrated luminosity of 35.9 fb^{-1} of proton-proton collisions at $\sqrt{s} = 13$ TeV collected with the CMS detector at the LHC in 2016. The analysis uses the invariant mass of the lepton pair, searching for a kinematic edge or a resonant-like excess compatible with the Z boson mass. The search for a kinematic edge targets strong production while the resonance search targets both strongly and electroweakly produced new physics. Both search modes use several event categories, based on observables related to the lepton pair and the hadronic system, in order to increase the sensitivity to new physics. A fit is also employed to search for a possible kinematic edge position in the strong, non-resonant search. The observations in all signal regions are consistent with the expectations from the standard model, and the results are interpreted in the context of simplified models of supersymmetry.

1 Introduction

Supersymmetry (SUSY) [1–8] is one of the most appealing extensions of the standard model (SM) and assumes a new fundamental symmetry that assigns a new fermion (boson) to every SM boson (fermion). SUSY resolves the hierarchy problem by stabilizing the Higgs boson mass via additional quantum loop corrections from the top super-partner (top squark), which compensate the correction due to the top quark. If R-parity [9] is conserved, the lightest state predicted by the theory is stable and potentially massive, providing a candidate for dark matter. Many SUSY models also lead to the unification of the electroweak and strong forces at high energies [10, 11].

This document presents a search for signatures of SUSY in events with two opposite-sign, same-flavor (OSSF) leptons (electrons or muons), jets, and missing transverse momentum. Searches for SUSY in this final state were performed previously by the CMS [12–17] and ATLAS [18–20] collaborations. The dataset of pp collisions used for the search was collected in 2016 with the CMS detector at the CERN LHC at $\sqrt{s} = 13\,\text{TeV}$ and corresponds to an integrated luminosity of 35.9 fb^{-1}. The dilepton topology is expected to occur in SUSY models where a neutralino decays to either an on-shell Z boson or a virtual Z/γ boson, which in turn decays to leptons and the lightest SUSY particle (LSP), or into a lepton and its supersymmetric partner (slepton), the latter decaying into another lepton and the LSP. Decays involving an on-shell Z boson are expected to produce an excess of events in which the dilepton invariant mass is compatible with the Z boson mass, while decays involving off-shell Z bosons or sleptons are expected to produce a characteristic edge shape in the invariant mass distribution of the dilepton system [21].

The search for a contribution at the Z boson mass is performed in both scenarios of strong and electroweak SUSY production and features corresponding signal models and event selections. In case of the strong production, the neutralino is part of a decay chain starting from a gluino or squark, while in the electroweak case it is directly produced. The search for a kinematic edge is only performed under the assumption of strongly produced SUSY.

2 The CMS detector

The central feature of the CMS apparatus is a superconducting solenoid, 13 m in length and 6 m in diameter, that provides an axial magnetic field of 3.8 T. The bore of the solenoid is outfitted with various particle detection systems. Charged-particle trajectories are measured by silicon pixel and strip trackers, covering $0 < \phi < 2\pi$ in azimuth and $|\eta| < 2.5$, where the pseudorapidity η is defined as $\eta = -\log[\tan(\theta/2)]$, with θ being the polar angle of the trajectory of the particle with respect to the beam direction. A crystal electromagnetic calorimeter (ECAL), and a brass and scintillator hadron calorimeter surround the tracking volume. The calorimeters provide energy and direction measurements of electrons and hadronic jets. Muons are measured in gas-ionization detectors embedded in the steel flux-return yoke outside the solenoid. The detector is nearly hermetic, allowing for energy balance measurements in the plane transverse to the beam direction. A two-tier trigger system selects the most interesting pp collision events for use in physics analysis. A more detailed description of the CMS detector, its coordinate system, and the main kinematic variables used in the analysis can be found elsewhere [22].

3 Datasets, triggers, and object selection

Events are collected with a set of dilepton triggers that require a transverse momentum of $p_T > 17$ or 23 GeV for the leading lepton depending on the data taking period, except for the dimuon trigger where the requirement is always $p_T > 17$ GeV. These triggers impose loose isolation criteria on the leptons. For the subleading electron (muon) $p_T > 12$ (8) GeV is required and both leptons have to satisfy $|\eta| < 2.5$ (2.4) for electrons (muons). In order to retain high signal efficiency, in particular for Lorentz-boosted dilepton systems, dilepton triggers without isolation requirement have been used, which require for both leptons $p_T > 33$ (30) GeV in the dielectron (electron muon) case and either $p_T > 27$ (8) GeV or $p_T > 30$ (11) GeV for the leading (subleading) muon in dimuon events. The trigger efficiencies are measured in data using events selected by a suite of hadronic triggers and are found to be 90–96%.

A particle flow (PF) technique [23, 24] is used to reconstruct particle candidates in the event. Electrons, reconstructed by associating tracks with ECAL clusters, are identified using a multivariate approach based on information on the cluster shape in the ECAL, track quality, and the matching between the track and the ECAL cluster [25]. Additionally, electrons from photon conversions are rejected. Muons are reconstructed from tracks found in the muon system associated with tracks found in the tracker. They are identified based on the quality of the track fit and the number of associated hits in the tracking detectors. For both lepton flavors, the impact parameter with respect to the reconstructed vertex with the largest p_T^2 sum of associated tracks (primary vertex) is required to be within 0.5 mm in the transverse plane and below 1 mm along the beam direction. The lepton isolation, defined as the scalar p_T sum of all particle flow candidates, excluding the lepton itself, in a cone around the lepton, divided by the lepton p_T, is required to be smaller than 0.1 (0.2) for electrons (muons). A cone-size, varying with lepton p_T, is chosen to be $\sqrt{\Delta\phi^2 + \Delta\eta^2} = \Delta R = 0.2$ for $p_T < 50$ GeV, $\Delta R = 10\,\text{GeV} / p_T$ for $50 < p_T < 200$ GeV, and $\Delta R = 0.05$ for $p_T > 200$ GeV. This shrinking cone-size as a function of p_T recovers leptons from highly boosted decays.

Photons are required to pass identification criteria [26], as well as have $p_T > 25$ GeV, and be within $|\eta| < 2.4$, excluding the transition region of $1.4 < |\eta| < 1.6$ between the ECAL barrel and endcap. Photons are required to be isolated from energy deposits within a cone of $\Delta R = 0.3$ and need to have an ECAL cluster shape consistent with the expectation for an electromagnetic shower. The fraction of energy deposited in the HCAL tower closest to the cluster seed in the ECAL has to be smaller than 5%, and photons need to have a non-zero shower width in the ECAL to veto spontaneous discharges of the ECAL avalanche photodiodes. To ensure the photon is well-measured, it is required that $\Delta\phi(\vec{p}_T^{\,\text{miss}}, \gamma) > 0.4$, and the photon must be matched to a jet within a cone of $\Delta R = 0.4$ where the electromagnetic fraction of this jet, i.e. the fraction of jet energy deposited in the electromagnetic calorimeter with respect to the total energy, is required to be > 0.7. Lastly, events are rejected if the photon can be connected to a pattern of hits in the pixel detector in order to distinguish photons from electrons.

Isolated, charged particles identified by the particle flow algorithm are used in some parts of the analysis. Particle flow candidates are identified with a looser set of criteria than the leptons above and are used as a veto on the presence of charged leptons. When selecting charged PF candidates a track–only isolation is used. Relative track isolation is calculated using all charged PF candidates within a cone $\Delta R < 0.3$ and longitudinal impact parameter $|\Delta z| < 0.1$ cm relative to the primary vertex. Particle flow candidates identified as electrons or muons (charged hadrons) are required to have $p_T > 5$ (10) GeV and an isolation value less than 0.2 (0.1) times the candidate p_T.

Jets are clustered from particle flow candidates, excluding charged hadrons not associated to

the primary vertex, using the anti-k_t clustering algorithm [27] implemented in the FASTJET package [28, 29] with a distance parameter of 0.4. Each jet is required to have $p_T > 35$ GeV where the p_T is corrected for non-uniform detector response and multiple collision (pileup) effects [30, 31], and $|\eta| < 2.4$. A jet is removed from the event if it lies within $\Delta R < 0.4$ of any of the selected leptons or the highest p_T photon. The scalar sum of all jet transverse momenta is referred to as H_T. The magnitude of the negative vector p_T sum of all the PF candidates is referred to as E_T^{miss}. Corrections to the jet energy are propagated to the E_T^{miss} using the procedure developed for 7 TeV data [30]. Identification of jets originating from b-quarks is performed with the combined secondary vertex algorithm, using the medium working point for which the typical efficiency for b quarks is around 60-75% and the mis-tagging rate for light-flavor jets is around 1.5% [32].

Events are selected by requiring two opposite-charge, same-flavor leptons ($e^{\pm}e^{\mp}$ or $\mu^{\pm}\mu^{\mp}$) with $p_T > 25$ (20) GeV for the leading (subleading) lepton and pseudorapidity $|\eta| < 2.4$ for both leptons. The distance between the leptons must satisfy $\Delta R > 0.1$ to avoid reconstruction efficiency differences between electrons and muons in events with very collinear leptons. To ensure symmetry in acceptance between electrons and muons, all leptons in the barrel-endcap transition region of the ECAL, $1.4 < |\eta| < 1.6$, are rejected. A control sample of leptons pairs with opposite charge but different flavor ($e^{\pm}\mu^{\mp}$) is defined using the same lepton selection criteria. All the parameters above have been chosen in order to maximize the lepton selection efficiency while keeping the electron and muon efficiencies similar. Photons are used to predict one of the main backgrounds of this analysis, and a control region in data made up of $\gamma +$ jets events is used for this. The p_T of the dilepton system is required to be greater than 25 GeV to be consistent with the thresholds for the photon in the $\gamma +$ jets control sample.

While the main SM backgrounds are estimated using data control samples, simulated events are used to estimate uncertainties and some SM background components. Next-to-leading order (NLO) and next-to-NLO cross sections [33–38] are used to normalize the simulated background samples, while NLO plus next-to-leading-logarithm (NLL) calculations [39–41] are used for the signal samples. Simulated samples of Drell-Yan (DY) processes or photons produced in associated with jets, are generated with the `MadGraph5_aMC@NLO` event generator [42] to leading order (LO) precision with up to four additional partons in the matrix element calculations. Simulated $t\bar{t}V$ ($V = W, Z$) and VVV events are produced with the same generator to NLO precision. Other SM processes, such as VV, $t\bar{t}$ and single top quark production are all simulated using `POWHEG` [43]. The matrix element calculations performed with these generators are interfaced with PYTHIA 8 [44] for the simulation of parton showering and hadronization. The NNPDF3.0 parton distribution functions (PDF) [45] are used for all samples. The detector response is simulated with a GEANT4 model [46] of the CMS detector. The simulation of new physics signals is performed using the `MadGraph5_aMC@NLO` program at LO precision with up to 2 additional partons in the matrix element calculations. Events are then interfaced with PYTHIA 8 for fragmentation and hadronization, and simulated using the CMS fast simulation package [47]. Multiple pp interactions are superimposed on the hard collision and the simulated samples are reweighted such that the number of collisions per bunch crossing accurately reflects what is seen in data. Normalization scale factors are applied to the simulated samples to account for differences between simulation and data in the trigger and reconstruction efficiencies.

4 Signal models

This search targets different production and decay modes within SUSY, all of which have a final state containing two opposite-sign, same-flavor leptons, jets, and E_T^{miss} originating from

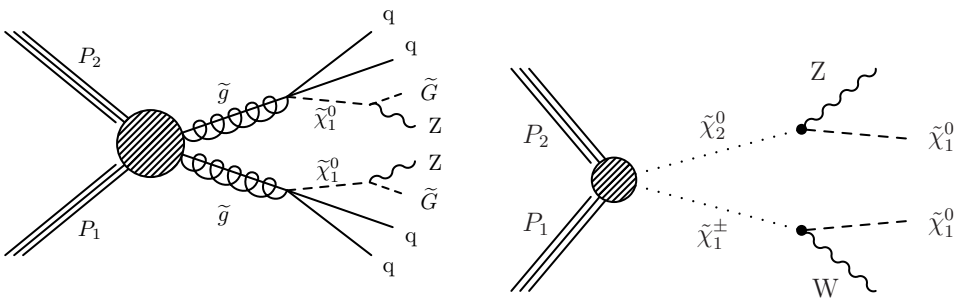

Figure 1: Diagrams for models with decays containing at least one dilepton pair stemming from a Z decay are shown. The gluino GMSB model targeted by the strong on-Z search is shown in the left. The right diagram shows the chargino-neutralino production model resulting in a final state with a Z boson, a W boson, and two LSPs. In the gluino GMSB model, $\tilde{G}$ denotes the massless gravitino.

the LSPs. Two primary signatures are considered and used to categorize the search regions. First, one neutralino is considered to decay into the LSP and an on-shell Z boson producing a resonant lepton signature in the final state. Second, the neutralino is considered to decay into the LSP and an off-shell Z boson, or into a pair of lepton-slepton, with the slepton decaying into another lepton and the LSP, both exhibiting an edge-like shape in the dilepton invariant mass distribution. These two decay modes will be referred as the "on-Z" signature and the "edge" signature.

The search targeting "on-Z" signatures is performed for strongly and electroweakly produced SUSY using signal regions designed to target different scenarios. The first simplified model used for interpretation of the on-Z signal regions assumes gauge mediated supersymmetry breaking (GMSB) [48–50]. It assumes strong production of a pair of gluinos ($\tilde{g}$) that each decay into a pair of quarks (u, d, s, c, or b) and the lightest neutralino, $\tilde{\chi}_1^0$. The $\tilde{\chi}_1^0$ in turn decays into a massless gravitino and a on-shell Z boson. This gluino GMSB model is shown in Fig. 1 (left).

The other model used for the on-Z search assumes electroweak production. The right diagram in Fig. 1 shows $\tilde{\chi}_1^\pm$-$\tilde{\chi}_2^0$ production, with $\tilde{\chi}_1^\pm$ decaying to a W boson and the LSP, $\tilde{\chi}_1^0$, while $\tilde{\chi}_2^0$ decays to a Z boson and $\tilde{\chi}_1^0$. The cross section used for this model assumes that the $\tilde{\chi}_1^\pm$ and $\tilde{\chi}_2^0$ are wino-like states. Gauge mediated supersymmetry breaking is not assumed for this model, and the $\tilde{\chi}_1^0$ is allowed to be massive. The Z and W bosons are always assumed to decay according to their SM branching fractions.

The signal model for the edge search, referred to as slepton-edge, assumes the production of a pair of bottom squarks, which decay to the next-to-lightest neutralino $\tilde{\chi}_2^0$ and a b quark. Two decay modes of the $\tilde{\chi}_2^0$ are considered each with 50% probability. In the first one, the $\tilde{\chi}_2^0$ decays to a Z boson and the lightest neutralino $\tilde{\chi}_1^0$, which is stable. The Z boson can be on- or off-shell, depending on the mass difference between the neutralinos, and decays according to its SM branching fractions. The second one features sequential two-body decays with an intermediate slepton $\tilde{\ell}$: $\tilde{\chi}_2^0 \to \tilde{\ell}\ell \to \ell\ell\tilde{\chi}_1^0$. The masses of the sleptons ($\tilde{e}$, $\tilde{\mu}$) are assumed degenerate and equal to the average of the $\tilde{\chi}_2^0$ and $\tilde{\chi}_1^0$. The masses of the $\tilde{b}$ and $\tilde{\chi}_2^0$ are free parameters, while $m_{\tilde{\chi}_1^0}$ is fixed at 100 GeV. This scheme allows the position of the signal edge to vary along the invariant mass distribution according to the mass difference between the $\tilde{\chi}_2^0$ and $\tilde{\chi}_1^0$. The mass of the $\tilde{\chi}_1^0$ has been chosen in such a way that the difference to the $\tilde{\chi}_2^0$ mass is above 50 GeV, setting the minimum possible edge position at 50 GeV. An example for one of the possible decays is shown in Fig. 2.

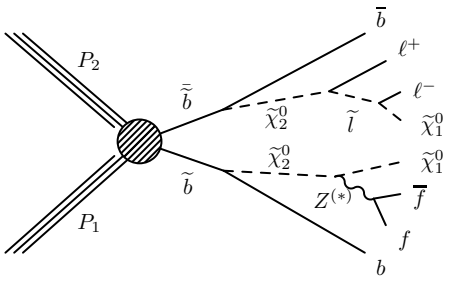

Figure 2: A diagram showing a model in which bottom squarks are pair produced with subsequent decays that contain at least one dilepton pair. This model features a characteristic edge in the $m_{\ell\ell}$ spectrum given approximately by the mass difference of the $\tilde{\chi}_2^0$ and $\tilde{\chi}_1^0$.

5 Signal Regions

The on-Z search regions are defined to achieve low expected backgrounds from SM processes while maintaining sensitivity to a variety of new physics models. These require dilepton invariant mass ($m_{\ell\ell}$) in the range $86 < m_{\ell\ell} < 96\,\text{GeV}$, $E_\text{T}^\text{miss} > 100\,\text{GeV}$, and at least 2 jets with $p_\text{T} > 35$ GeV. Events with additional electrons (muons) with an isolation of 0.4, $p_\text{T} > 10$ GeV and $|\eta| < 2.5$ (2.4) are rejected, as are events containing an isolated, charged PF candidate passing the selections described above. The two highest p_T jets in the event are required to have a separation in ϕ from E_T^miss of at least 0.4 to reduce backgrounds where the E_T^miss in the event comes from jet mismeasurements. These selection criteria serve as a baseline for all the on-Z search regions, and then three separate regions are defined, one for the strong search, and two for electroweak searches.

For the strong search region, we make selections requiring large amounts of hadronic activity in the event, which we expected in the decays of strongly-coupled new particles. We define three signal region categories (SR): "SRA" (2–3 jets), "SRB" (4–5 jets), and "SRC" ($\geq$ 6 jets). These categories are further divided as either having 0 or at least one b-tagged jet with $p_\text{T} > 25\,\text{GeV}$. The kinematic variable M_T2 [51, 52] was originally introduced to measure the mass of pair-produced particles decaying to the same visible and invisible particle. When building M_T2 from both leptons and E_T^miss, denoted $\text{M}_\text{T2}(\ell\ell)$, the distribution exhibits a sharp decline around the mass of the W boson for $\text{t}\bar{\text{t}}$ events and is therefore well suited to suppress its contributions. A requirement of $\text{M}_\text{T2}(\ell\ell) > 80$ (100 for events with at least 1 b-tagged jet) GeV is imposed in order to suppress $\text{t}\bar{\text{t}}$ backgrounds. Requirements are then placed on H_T depending on the number of jets and on the presence or not of a b-tagged jet in the event.

The first electroweak search region is designed to be sensitive to signatures where a W or Z boson is produced in conjunction with the leptonically decaying Z boson. In order to reduce the $\text{t}\bar{\text{t}}$ background, events with a b-tagged jet are removed, and we require $\text{M}_\text{T2}(\ell\ell) > 80$ GeV. The two jets in the event that are closest in ϕ are then required to have an invariant mass $\text{m}_\text{jj} < 110$ GeV to be consistent with the hadronic decay of a W or Z boson. The signal region is then divided into four bins in E_T^miss: 100 – 150 GeV, 150 – 250 GeV, 250 – 350 GeV, and above 350 GeV.

The second electroweak search region is designed to be sensitive to signatures where a Higgs boson is produced in conjunction with the leptonically decaying Z boson. We require the Higgs boson to decay to $\text{b}\bar{\text{b}}$, and we therefore require events to have exactly two b-tagged jets with an invariant mass, m_bb, less than 150 GeV. In order to reduce the $\text{t}\bar{\text{t}}$ background, an M_T2 variable is calculated using a combination of the two leptons and two b jets as the visible objects.

Each lepton is paired together with a b jet, and all combinations of M_{T2} are calculated. The lowest value of M_{T2} is used, denoted $M_{T2}(\ell b \ell b)$, and is required to be less than 200 GeV. The signal region is then divided into three bins in E_T^{miss}: 100 – 150 GeV, 150 – 250 GeV, and above 250 GeV.

The baseline signal region in the edge search requires $m_{\ell\ell} > 20$ GeV, at least two jets, $E_T^{miss} > 150$ GeV, $M_{T2} > 80$ GeV and the two highest p_T jets to have a separation in ϕ from E_T^{miss} of at least 0.4. The fit to search for a kinematic edge in the invariant dilepton mass spectrum is performed in this baseline region. To perform a counting experiment, this region is further subdivided into seven $m_{\ell\ell}$ regions, excluding the range used for the on-Z search. These are summarized in Table 1.

A likelihood discriminant is used to distinguish between events originating from dileptonically decaying top quark pairs and the rest. The observables used for the likelihood discriminator are: E_T^{miss}, the p_T of the dilepton system, $|\Delta(\phi)|$ between the leptons, and an observable called $\Sigma m_{\ell b}$. The latter is the sum of the invariant masses of the two lepton and b-jet systems, and should have an endpoint at two times the mass of the top quark for events with top quark pairs. To calculate $\Sigma m_{\ell b}$, all combinations of leptons and jets are selected and the minimum mass is found. This process is repeated for the remaining lepton and jets, and the sum of the masses of the two systems is then defined as $\Sigma m_{\ell b}$. If b-tagged jets are present, they are given priority in the calculation of both lepton-jet systems; i.e. if one or two (or more) b-jets are present, $\Sigma m_{\ell b}$ between the leptons and the b-jets is minimized first, and then the remaining (b-)jets are considered for the minimization of the sum $\Sigma m_{\ell b}$ of the second lepton. To calculate this likelihood, the probability density functions of the four observables are determined by fits in the opposite-flavor control sample using the same kinematic requirements as the same-flavor signal region except the M_{T2} selection. The respective fit functions are a sum of two exponentials for the E_T^{miss}, a second-order polynomial for the $|\Delta(\phi)|$, and a Crystal-Ball function for both the dilepton p_T as well as the $\Sigma m_{\ell b}$ distribution. A likelihood function is then constructed and its negative logarithm is taken as the discriminator value. Two categories of events are then defined, namely events that are $t\bar{t}$-like and those that are non-$t\bar{t}$-like. A discriminator value of 21 is chosen to have an efficiency of 95% and 5% for the two categories.

In addition, two aggregate signal regions have been defined for the edge search, integrating the mass bins below and above the Z boson mass for the non-$t\bar{t}$-like category.

The selections for all signal regions are summarized in Table 1.

6 Standard model background predictions

The backgrounds from SM processes are divided into three types. Those that produce opposite-flavor (OF) pairs ($e^{\pm}\mu^{\mp}$) as often as same-flavor (SF) pairs ($\mu^{\pm}\mu^{\mp}$, $e^{\pm}e^{\mp}$) are referred to as flavor-symmetric (FS) backgrounds. Among them, the dominant contribution arises from top quark pair production; sub-leading contributions from W^+W^-, $Z/\gamma^*(\rightarrow \tau\tau)$, tW single-top quark production, and leptons from hadron decays are also present. The next categories of backgrounds include flavor-correlated lepton production and only contributes with SF leptons. The dominant contributions at lower E_T^{miss} arise from DY production in association with jets, where the E_T^{miss} arises from mismeasurement of the jet energies. Other contributions come from WZ and ZZ production, as well as rare processes such as $t\bar{t}Z$, which can have prompt neutrinos in addition to an OSSF pair from Z/γ^*. These backgrounds are referred to as "Other SM" in this document and can be important in the high E_T^{miss} signal bins.

Table 1: Summary of all signal region selections.

Strong on-Z Signal Regions					
Region	N_{jets}	$N_{\text{b-jets}}$	H_{T}	$\text{M}_{\text{T2}}(\ell\ell)$	$E_{\text{T}}^{\text{miss}}$ binning [GeV]
SRA b-veto	2–3	= 0	$>$ 500 GeV	$>$ 80 GeV	[100,150,250,∞]
SRB b-veto	4–5	= 0	$>$ 500 GeV	$>$ 80 GeV	[100,150,250,∞]
SRC b-veto	$\geq$ 6	= 0	-	$>$ 80 GeV	[100,150,∞]
SRA b-tag	2–3	$\geq$ 1	$>$ 200 GeV	$>$ 100 GeV	[100,150,250,∞]
SRB b-tag	4–5	$\geq$ 1	$>$ 200 GeV	$>$ 100 GeV	[100,150,250,∞]
SRC b-tag	$\geq$ 6	$\geq$ 1	-	$>$ 100 GeV	[100,150,∞]
Electroweak on-Z Signal Regions					
Region	N_{jets}	$N_{\text{b-jets}}$	dijet mass	M_{T2}	$E_{\text{T}}^{\text{miss}}$ binning [GeV]
VZ	$\geq$ 2	= 0	$\text{m}_{\text{jj}} < 110$ GeV	$\text{M}_{\text{T2}}(\ell\ell) > 80$ GeV	[100,150,250,350,∞]
HZ	$\geq$ 2	= 2	$\text{m}_{\text{bb}} < 150$ GeV	$\text{M}_{\text{T2}}(\ell b \ell b) > 200$ GeV	[100,150,250,∞]
Edge Signal Regions					
Region	N_{jets}	$E_{\text{T}}^{\text{miss}}$	$\text{M}_{\text{T2}}(\ell\ell)$	$\text{t}\bar{\text{t}}$ likelihood	$m_{\ell\ell}$ binning [GeV]
Edge Fit	$\geq$ 2	$>$ 150 GeV	$>$ 80 GeV	-	$>$ 20
$\text{t}\bar{\text{t}}$ like	$\geq$ 2	$>$ 150 GeV	$>$ 80 GeV	$<$ 21	[20,60,86],[96,150,200,300,400,∞]
non-$\text{t}\bar{\text{t}}$ like	$\geq$ 2	$>$ 150 GeV	$>$ 80 GeV	$>$ 21	[20,60,86],[96,150,200,300,400,∞]

6.1 Flavor-symmetric backgrounds

The method of estimating the FS backgrounds relies on the fact that for such processes, SF and OF are produced at the same rate at particle level. This allows for prediction of the background yields in the SF sample from those of the OF sample by application of an appropriate translation factor estimated from control regions in data. For cases where the OF contribution is of sufficient statistical power to make an accurate prediction in the SF channel, this translation factor corrects for different flavor-dependent reconstruction and identification efficiencies, and from flavor-dependent trigger efficiencies, which might be different for electrons and muons.

A background estimate in the SF channel can therefore be obtained by applying a multiplicative correction factor, $R_{\text{SF/OF}}$, to the OF channel yield. This factor is determined in two independent ways: purely on collision data and then using the weighted average of the two independent measurements according to their uncertainties. One approach uses a direct measurement of this translation factor in a control region outside of the baseline signal region, and the second involves a factorized approach of measuring the effects of reconstruction, identification, and trigger separately.

The direct measurement is performed in the region with $N_{\text{jets}} = 2$ and $100 < E_{\text{T}}^{\text{miss}} < 150\,\text{GeV}$, excluding the mass range $70 < m_{\ell\ell} < 110\,\text{GeV}$ to reduce contributions from DY backgrounds. Here, $R_{\text{SF/OF}}$ is evaluated using the observed yield of SF and OF events, $R_{\text{SF/OF}} = \text{N}_{\text{SF}}/\text{N}_{\text{OF}}$. A validation is performed in $\text{t}\bar{\text{t}}$ simulated events in the signal region where the obtained values of $R_{\text{SF/OF}}$ differs by 1% with respect to the value obtained in data. Further dependencies of $R_{\text{SF/OF}}$ on the most relevant observables of the analysis are also checked and a systematic uncertainty of 4% is assigned to cover for them. The measured value of $R_{\text{SF/OF}}$ is 1.107$\pm$0.046.

For the factorized approach, the ratio of muon to electron reconstruction and identification efficiencies, $r_{\mu/\text{e}}$, is measured in a DY-enriched region with $N_{\text{jets}} \geq 2$ and $E_{\text{T}}^{\text{miss}} < 50\,\text{GeV}$ and requiring $60 < m_{\ell\ell} < 120\,\text{GeV}$. This results in a large sample of $\text{e}^{\pm}\text{e}^{\mp}$ and $\mu^{\pm}\mu^{\mp}$ events with similar kinematics to the signal region in terms of jet multiplicity. Assuming the factorization of lepton efficiencies in an event, the efficiency ratio is measured as $r_{\mu/\text{e}} = \sqrt{\text{N}_{\mu^+\mu^-}/\text{N}_{\text{e}^+\text{e}^-}}$. This ratio depends on the lepton p_{T} and a parameterization as a function of the p_{T} of the less energetic lepton is chosen:

$$r_{\mu e} = r_{\mu e,c} + \frac{\alpha}{p_{\mathrm{T}}}$$

Here $r_{\mu e,c}$ and α are constants that are determined in a fit to data and cross checked on MC. These fit parameters are determined to be $r_{\mu e,c}$ = 1.140±0.005 and α = 5.20±0.16. A 10% systematic uncertainty is assessed in order to cover for the deviations observed when studying the dependence of $r_{\mu/\mathrm{e}}$ on the $E_{\mathrm{T}}^{\mathrm{miss}}$ and the jet multiplicity.

The trigger efficiencies for the three different flavor combinations are used to define the factor $R_{\mathrm{T}} = \sqrt{\epsilon^{T}_{\mu^{\pm}\mu^{\mp}}\epsilon^{T}_{\mathrm{e}^{\pm}\mathrm{e}^{\mp}}}/\epsilon^{T}_{e^{\pm}\mu^{\mp}}$, which takes into account the difference between SF and OF channels at the trigger level. The efficiencies are estimated from a control sample of events collected with a set of orthogonal triggers and range from 90 to 96%, yielding a final value of R_{T} = 1.052±0.043.

The final correction is $R_{\mathrm{SF/OF}} = \frac{1}{2}(r_{\mu/\mathrm{e}} + r^{-1}_{\mu/\mathrm{e}}) \cdot \mathrm{R_T}$. Here, $r_{\mu/\mathrm{e}}$ is summed with its inverse, leading to a large reduction of the associated uncertainty. Since $r_{\mu/\mathrm{e}}$ depends on the lepton kinematics, this correction is done on an event-by-event basis. A separate correction is determined for each signal region and combined with the correction from the direct measurement using the weighted average.

6.1.1 Adaptations to the FS background prediction for on-Z regions

The FS method described above is designed for signal regions where the expected number of background events from FS processes is expected to be large due to the fact that the statistical uncertainty on the predicted number of events is driven by the statistical uncertainty on the number of events in the OF control region. The requirement of $m_{\ell\ell}$ to be within 5 GeV of the Z boson mass in the on-Z regions reduces the FS background by a significant amount, such that the expected yields in several bins are on the order of a few events or less. We therefore modify the method to obtain greater statistical power by relaxing the cut on $m_{\ell\ell}$ for OF events. This increases the number of events in the OF control region. An additional multiplicative factor, κ, is calculated and multiplied together with $R_{\mathrm{SF/OF}}$ in order to translate this into a prediction for the SF signal region. The factor κ is defined as the number of OF events with $|m_Z - m_{\ell\ell}| < 5$ GeV divided by the number of events in the whole OF sample. It is determined from the OF control sample from simulation and validated in the respective data control regions. A value for κ of 0.065 is measured in MC, and data is seen to agree well with this value. A systematic uncertainty of 30% is chosen by computing κ from simulated events for the various on-Z signal regions and in bins of $E_{\mathrm{T}}^{\mathrm{miss}}$ and taking the largest observed difference from the nominal κ value. The statistical uncertainty of κ is negligible in comparison with the systematic uncertainty.

6.2 Drell-Yan+jets backgrounds

6.2.1 $E_{\mathrm{T}}^{\mathrm{miss}}$ template method

The $E_{\mathrm{T}}^{\mathrm{miss}}$ from the DY background is estimated from $E_{\mathrm{T}}^{\mathrm{miss}}$ templates obtained from a data control region. The main premise of this estimate based on data is that $E_{\mathrm{T}}^{\mathrm{miss}}$ in Z + jets events originates from the limited detector resolution when measuring the objects making up the hadronic system that recoils against the Z boson. The shape of the $E_{\mathrm{T}}^{\mathrm{miss}}$ distribution is estimated from a control sample of γ + jets events where the jet system recoils against a photon instead of a Z boson. Signal regions requiring at least one b-tagged jet can lead to a small amount of additional $E_{\mathrm{T}}^{\mathrm{miss}}$ due to the neutrinos in semileptonic b quark decays. To account for this effect, the

$E_{\mathrm{T}}^{\mathrm{miss}}$ templates are extracted from a control sample of γ + jets events with the same b-tagging requirement.

The γ+ jets events in data are selected with a suite of single-photon triggers with p_{T} thresholds varying from 22 to 165 GeV. The triggers with thresholds below 165 GeV are prescaled such that only a fraction of accepted events are recorded, and the events are weighted by the trigger prescales to match the integrated luminosity collected with the signal dilepton triggers. In order to account for kinematic differences between the hadronic systems in the γ + jets and the Z + jets samples, the γ + jets sample is reweighted such that the boson p_{T} distribution matches that of the Z + jets sample. This reweighting is performed for each signal region, where the same requirements are applied to the Z + jets and the γ + jets samples.

The variable $\mathrm{M_{T2}}$ used in the signal region requires two visible objects as input, whereas the single photon in the γ + jets does not meet this requirement. Therefore, the template method was adapted to allow for this cut on $\mathrm{M_{T2}}$ by developing a procedure to emulate this cut in γ + jets by decaying the photon to two leptons. This procedure is described in detail in section 6.2.2. The resulting $E_{\mathrm{T}}^{\mathrm{miss}}$ distribution is then normalized to the observed data yield for each signal region in the range $50 < E_{\mathrm{T}}^{\mathrm{miss}} < 100$ GeV, where Z + jets is the dominant background.

6.2.2 $\mathrm{M_{T2}}$ emulation for the $E_{\mathrm{T}}^{\mathrm{miss}}$-template method

Two visible objects are needed when calculating the $\mathrm{M_{T2}}$ variable, and only one photon is required in the γ + jets events used to predict the $E_{\mathrm{T}}^{\mathrm{miss}}$ from the Z + jets background in the signal regions. Therefore in order to emulate the $\mathrm{M_{T2}}$ cut in the γ + jets sample, a method was developed where the photon is decayed to two leptons, and $\mathrm{M_{T2}}(\ell\ell)$ is calculated using the two decayed leptons as the visible objects. This decay is done by assuming the mother particle has the mass of a Z boson and the momentum of the photon reconstructed from data. The angular distribution of the leptons is accounted for by assuming a scenario where the direction of the spin of the mother particle is sampled from a distribution that is flat in $(1 + \cos^2(\theta))$, where θ is the polar angle in the rest frame of the mother particle. After the photon is decayed, the same p_{T} and η requirements that are applied to the Z + jets events are applied to the decay products from the photon. $\mathrm{M_{T2}}(\ell\ell)$ is constructed using these leptons, and the same cut is applied to $\mathrm{M_{T2}}(\ell\ell)$ depending on the signal region.

6.2.3 Correcting electroweak contamination in tails of $E_{\mathrm{T}}^{\mathrm{miss}}$ templates

After selecting events with a high-p_{T} photon and large $E_{\mathrm{T}}^{\mathrm{miss}}$, events from electroweak processes with real $E_{\mathrm{T}}^{\mathrm{miss}}$, e.g. W$\gamma$ where the W boson decays to $\ell\nu$, can be present in the tail of the $E_{\mathrm{T}}^{\mathrm{miss}}$ distribution. A cut is applied to the γ + jets data sample vetoing events that contain a lepton to reduce the contamination from these electroweak processes, where the lepton has the same definition as the veto lepton used in the signal selection. We then subtract the residual electroweak contamination after applying this selection, and the predicted value of this contamination is taken from simulation after applying all the same selections, including the aforementioned lepton veto.

To examine the modeling of these processes, we define a control region by selecting events with exactly one muon and one photon, requiring $E_{\mathrm{T}}^{\mathrm{miss}} > 50$ GeV and the transverse mass of the muon and the $E_{\mathrm{T}}^{\mathrm{miss}}$, M_T, to be greater than 30 GeV. We collect these events using an isolated single muon trigger that has a p_{T} requirement of 24 GeV online, and we select muons with $p_{\mathrm{T}} > 25$ GeV offline. This region consists of about 50% Wγ events with the remainder coming primarily from $\mathrm{t\bar{t}}\gamma$ events. Agreement is observed between data and the prediction from simulation. Based on the modeling of the kinematic distributions of photon p_{T} and $E_{\mathrm{T}}^{\mathrm{miss}}$,

we assign a systematic uncertainty of 30% on the subtraction of these electroweak processes.

6.2.4 Systematic uncertainties of the $E_{\mathrm{T}}^{\mathrm{miss}}$ template method

The systematic uncertainty in the prediction takes into account the statistical uncertainty of the γ + jets sample in the signal $E_{\mathrm{T}}^{\mathrm{miss}}$ regions. The statistical uncertainty of the normalization for $E_{\mathrm{T}}^{\mathrm{miss}} < 50$ GeV is included and ranges from 7–30%. A closure test of the method is performed in simulation, using γ + jets to predict the yield of Z + jets. An uncertainty is assigned from the results of this test as either the difference between the γ + jets prediction and the Z + jets yield for each $E_{\mathrm{T}}^{\mathrm{miss}}$ region, or the simulation statistical uncertainty, whichever is larger. The values vary between 10–80%, depending on the $E_{\mathrm{T}}^{\mathrm{miss}}$ region. We also take a 30% uncertainty on the subtraction of electroweak processes with genuine $E_{\mathrm{T}}^{\mathrm{miss}}$ from the γ + jets sample.

6.2.5 Drell–Yan background in the edge search

A procedure was designed to propagate the estimations obtained using the $E_{\mathrm{T}}^{\mathrm{miss}}$ templates from the on-Z regions to the edge signal regions. A ratio $r_{\mathrm{out/in}}$ is measured in the DY-dominated control region with $N_{\mathrm{jets}} \geq 2$, $E_{\mathrm{T}}^{\mathrm{miss}} < 50$ GeV, and $\mathrm{M_{T2}} > 80$ GeV. The numerator is the number of SF events outside of the Z boson mass window, while the denominator is the SF yield within this window. Opposite-flavor yields in both the numerator and denominator are subtracted from the respective same-flavor yields in order to correct for FS contributions in the region where $r_{\mathrm{out/in}}$ is measured. The value of $r_{\mathrm{out/in}}$ ranges from 0.1 % to 16 % for the different mass regions. The Z + jets background contribution to the edge signal regions is then the on-Z prediction multiplied by this ratio for each of the signal regions. Further dependencies of $r_{\mathrm{out/in}}$ on $E_{\mathrm{T}}^{\mathrm{miss}}$ and the jet multiplicity are studied and an uncertainty of 50 (100) % is assigned for mass bins below (above) 150 GeV to cover for deviations, considering also the limited statistics available for this study after applying the $\mathrm{M_{T2}}$ requirement.

6.3 Other SM: backgrounds with a Z boson and genuine MET

The $E_{\mathrm{T}}^{\mathrm{miss}}$ template method only predicts instrumental $E_{\mathrm{T}}^{\mathrm{miss}}$ from jet mismeasurement and thus does not include the genuine $E_{\mathrm{T}}^{\mathrm{miss}}$ from neutrinos expected in processes like W($\ell\nu$)Z ($\ell\ell$), Z ($\ell\ell$)Z ($\nu\nu$), or rarer processes such as $\mathrm{t\bar{t}Z}$. These processes can be a substantial fraction of the background at high $E_{\mathrm{T}}^{\mathrm{miss}}$ are estimated with simulation, and are also referred to as "Rares".

The prediction from simulation is validated by comparing to data in 3- and 4-lepton control regions. A region enriched in WZ events is selected by requiring exactly 3 leptons, $N_{\mathrm{jets}} \geq 2$, $E_{\mathrm{T}}^{\mathrm{miss}} > 60$ GeV, $N_{\text{b-jets}} = 0$, and an OSSF lepton pair with $86 < m_{\ell\ell} < 96$ GeV. Another 3-lepton control region is defined targeting $\mathrm{t\bar{t}Z}$ by requiring $N_{\mathrm{jets}} \geq 2$, $E_{\mathrm{T}}^{\mathrm{miss}} > 30$ GeV, $N_{\text{b-jets}} \geq 2$, and an OSSF lepton pair as in the WZ region. A 4-lepton control region targeting ZZ is constructed by requiring 4 leptons with both pairs satisfying $m_{\ell\ell} > 20$ GeV to remove low-mass resonances and $N_{\mathrm{jets}} \geq 2$.

After subtracting the other processes using simulation in each region, data/simulation scale factors of 0.98 ± 0.11, 1.58 ± 0.49, and 1.31 ± 0.29 are observed for WZ, ZZ, and $\mathrm{t\bar{t}Z}$ respectively. We use the scale factor values to correct the prediction from simulation for each process and take a conservative 30% uncertainty for the WZ and $\mathrm{t\bar{t}Z}$ samples and 50% for ZZ.

7 Kinematic fit

The search for a kinematic edge in the $m_{\ell\ell}$ distribution using shape information involves a simultaneous extended unbinned maximum likelihood fit to the dilepton mass distributions

of e^+e^-, $\mu^+\mu^-$, and $e^\pm\mu^\mp$ events. The likelihood model contains three components: a) a FS background component, b) a DY background component, and c) a signal component.

The FS background component is described using a Crystal-Ball [53] function: $\mathcal{P}_{CB}(m_{\ell\ell})$:

$$\mathcal{P}_{CB}(m_{\ell\ell}) = \begin{cases} \exp\left(-\frac{(m_{ll}-\mu_{CB})^2}{2\sigma_{CB}^2}\right) & \text{if } \frac{m_{ll}-\mu_{CB}}{\sigma_{CB}} < \alpha, \\ A(B+\frac{m_{ll}-\mu_{CB}}{\sigma_{CB}})^{-n} & \text{if } \frac{m_{ll}-\mu_{CB}}{\sigma_{CB}} > \alpha, \end{cases} \tag{1}$$

where

$$A = \left(\frac{n}{|\alpha|}\right)^n \exp\left(-\frac{|\alpha|^2}{2}\right) \quad \text{and} \quad B = \frac{n}{|\alpha|} - |\alpha|. \tag{2}$$

The FS background model has five free parameters: the overall normalization, the mean μ_{CB} and width σ_{CB} of the Gaussian part, the transition point α between the Gaussian part and the power law tail, and the power law parameter n.

The DY background component is modeled with the sum of an exponential function, which describes the low-mass rise, and a Breit–Wigner function with a mean and width set to the nominal Z boson values [54], which accounts for the on-Z lineshape. To account for the experimental resolution, the Breit–Wigner function is convolved with a double-sided Crystal-Ball [53] function $\mathcal{P}_{DSCB}(m_{\ell\ell})$:

$$\mathcal{P}_{DSCB}(m_{\ell\ell}) = \begin{cases} A_1(B_1 - \frac{m_{ll}-\mu_{DSCB}}{\sigma_{DSCB}})^{-n_1} & \text{if } \frac{m_{ll}-\mu_{DSCB}}{\sigma_{DSCB}} < -\alpha_1, \\ \exp\left(-\frac{(m_{ll}-\mu_{DSCB})^2}{2\sigma_{DSCB}^2}\right) & \text{if } -\alpha_1 < \frac{m_{ll}-\mu_{DSCB}}{\sigma_{DSCB}} < \alpha_2, \\ A_2(B_2 + \frac{m_{ll}-\mu_{DSCB}}{\sigma_{DSCB}})^{-n_2} & \text{if } \frac{m_{ll}-\mu_{DSCB}}{\sigma_{DSCB}} > \alpha_2, \end{cases} \tag{3}$$

The full model for the on-Z DY lineshape is thus:

$$\mathcal{P}_{DY,\,\text{on-Z}}(m_{\ell\ell}) = \int \mathcal{P}_{DSCB}(m_{\ell\ell})\mathcal{P}_{BW}(m_{\ell\ell} - m')dm'. \tag{4}$$

The signal component is described by a triangular shape, convolved with a Gaussian distribution to account for the experimental resolution:

$$\mathcal{P}_S(m_{\ell\ell}) \propto \frac{1}{\sqrt{2\pi}\sigma_{\ell\ell}} \int_0^{m_{\ell\ell}^{edge}} y \cdot \exp\left(-\frac{(m_{\ell\ell}-y)^2}{2\sigma_{\ell\ell}^2}\right) dy. \tag{5}$$

As a first step, a fit is performed separately for electrons and muons in the DY-enriched control region with $N_{\text{jets}} \geq 2$ and $E_{\text{T}}^{\text{miss}} < 50\,\text{GeV}$ to determine the shape of backgrounds containing a Z boson. The parameters of the DY shape are then fixed and only the normalizations of these backgrounds are free parameters in the fit. The final fit is performed simultaneously to the dilepton invariant mass distributions in the e^+e^-, $\mu^+\mu^-$, and $e^\pm\mu^\mp$ samples in the baseline signal region. Therefore the model for the FS background is the same for the SF and OF events.

The $R_{\text{SF/OF}}$ factor is treated as a nuisance parameter, parameterized by Gaussian distributions with a mean value and standard deviation given by the value of $R_{\text{SF/OF}}$ and its uncertainties (see Section 6.1).

The signal model has two free parameters: the fitted signal yield and the position of the edge.

8 Results

The observed number of events in the signal regions is compared with the background estimates obtained with the methods described previously for the strong and electroweak on-Z searches and the edge searches. The covariance and correlation matrices of the background predictions in the different signal regions are also provided in appendix A. For the edge search, the fit is performed to search for a kinematic edge in the $m_{\ell\ell}$ spectrum.

8.1 Results of the search in the on-Z signal regions

The results for the signal regions of the strong on-Z search are presented in Table 2. The corresponding $E_{\mathrm{T}}^{\mathrm{miss}}$ distributions are shown in Fig. 3. No significant excess of observation with respect to expectation is observed.

Table 2: Predicted and observed event yields are shown for the strong on-Z signal regions, for each region and $E_{\mathrm{T}}^{\mathrm{miss}}$ bin defined in Table 1. The uncertainties shown include both statistical and systematic errors.

SRA	$E_{\mathrm{T}}^{\mathrm{miss}}$ [GeV]	50-100	100-150	150-250	250+
	Template	208.5±16.1	13.6±3.1	2.5±0.9	3.3±2.4
	FS	$0.4^{+0.3}_{-0.2}$	$0.4^{+0.3}_{-0.2}$	$0.2^{+0.2}_{-0.1}$	$0.2^{+0.2}_{-0.1}$
	Rares	1.1±0.4	0.8±0.3	1.4±0.4	2.4±0.8
	Sum	210.0±16.1	14.8±3.2	4.0±1.0	5.9±2.5
	Data	210	23	5	4
SRAb	$E_{\mathrm{T}}^{\mathrm{miss}}$ [GeV]	50-100	100-150	150-250	250+
	Template	92.2±10.4	8.2±2.1	1.2±0.5	0.5±0.3
	FS	1.9±0.7	2.3±0.8	$1.7^{+0.7}_{-0.6}$	$0.1^{+0.2}_{-0.1}$
	Rares	1.9±0.4	1.9±0.4	2.0±0.5	1.8±0.6
	Sum	96.0±10.4	12.4±2.3	4.9±1.0	2.5±0.7
	Data	96	14	7	1
SRB	$E_{\mathrm{T}}^{\mathrm{miss}}$ [GeV]	50-100	100-150	150-250	250+
	Template	130.1±12.8	12.8±2.3	0.9±0.3	0.4±0.2
	FS	0.3±0.2	$0.4^{+0.3}_{-0.2}$	$0.4^{+0.3}_{-0.2}$	$0.1^{+0.2}_{-0.1}$
	Rares	0.6±0.2	0.3±0.1	0.7±0.2	1.2±0.4
	Sum	131.0±12.8	13.6±2.4	2.0±0.5	$1.6^{+0.5}_{-0.4}$
	Data	131	10	4	0
SRBb	$E_{\mathrm{T}}^{\mathrm{miss}}$ [GeV]	50-100	100-150	150-250	250+
	Template	37.9±6.7	7.7±3.1	4.0±3.3	0.1±0.1
	FS	$0.7^{+0.4}_{-0.3}$	$1.4^{+0.6}_{-0.5}$	$1.1^{+0.5}_{-0.4}$	$0.2^{+0.2}_{-0.1}$
	Rares	1.3±0.4	2.0±0.5	2.3±0.6	1.0±0.3
	Sum	40.0±6.8	11.1±3.2	7.4±3.4	$1.3^{+0.4}_{-0.3}$
	Data	40	10	5	0
SRC	$E_{\mathrm{T}}^{\mathrm{miss}}$ [GeV]	50-100	100-150	150+	
	Template	23.8±5.5	1.2±0.4	0.1±0.1	
	FS	$0.1^{+0.2}_{-0.1}$	$0.4^{+0.3}_{-0.2}$	$0.1^{+0.2}_{-0.1}$	
	Rares	0.2±0.1	0.1±0.1	0.5±0.2	
	Sum	24.0±5.5	1.7±0.5	$0.7^{+0.3}_{-0.2}$	
	Data	24	4	0	
SRCb	$E_{\mathrm{T}}^{\mathrm{miss}}$ [GeV]	50-100	100-150	150+	
	Template	9.9±3.7	0.1±0.5	0.0±0.3	
	FS	$0.1^{+0.2}_{-0.1}$	$0.0^{+0.1}_{-0.0}$	0.3±0.2	
	Rares	0.0±0.1	0.6±0.2	0.6±0.2	
	Sum	10.0±3.7	0.8±0.5	$0.9^{+0.5}_{-0.4}$	
	Data	10	2	2	

The results for the electroweak signal regions in the on-Z search are shown in Table 3. The corresponding $E_{\mathrm{T}}^{\mathrm{miss}}$ distributions are shown in Fig. 4. Here the observed data are also consistent with the background prediction.

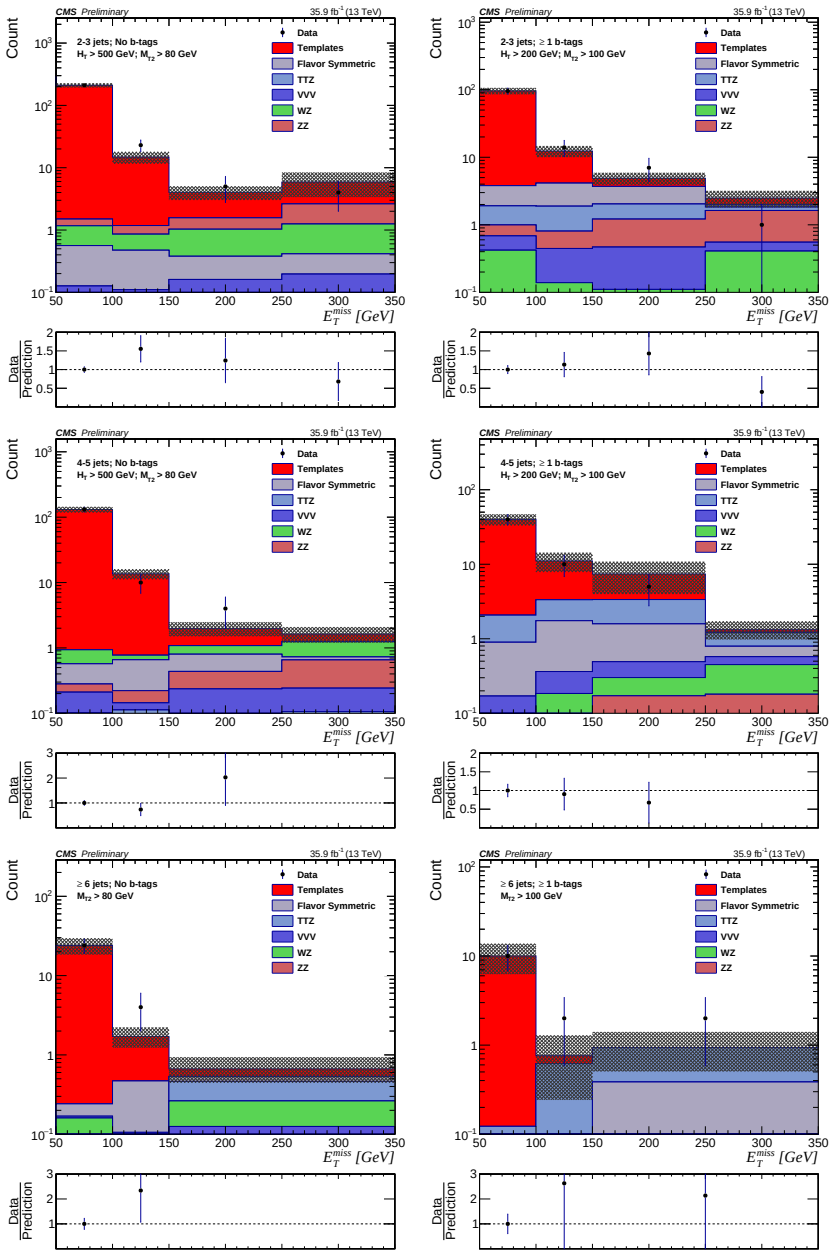

Figure 3: The $E_{\mathrm{T}}^{\mathrm{miss}}$ distribution is shown for data compared to the background prediction in the strong on-Z signal regions with $N_{\text{b-jets}} = 0$ (left) and $N_{\text{b-jets}} \geq 1$ (right). The rows show SRA (top), SRB (middle), and SRC (bottom). The $E_{\mathrm{T}}^{\mathrm{miss}}$ template prediction for each signal region is normalized to the first bin of each distribution, and therefore the prediction agrees with the data by construction.

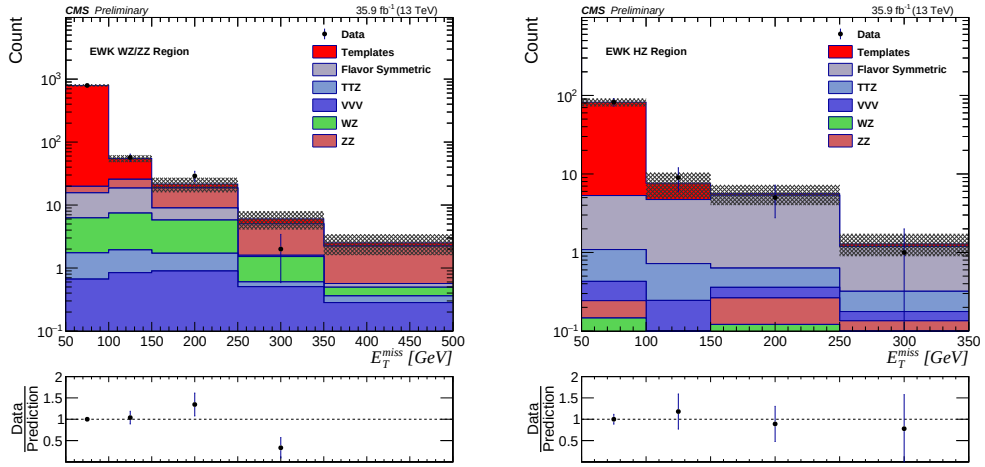

Figure 4: The $E_{\mathrm{T}}^{\mathrm{miss}}$ distribution is shown for data compared to the background prediction in the electroweak on-Z WZ/ZZ (left), and HZ (right) signal regions. The $E_{\mathrm{T}}^{\mathrm{miss}}$ template prediction for each signal region is normalized to the first bin of each distribution, and therefore the prediction agrees with the data by construction.

Table 3: Predicted and observed event yields are shown for the electroweak on-Z signal regions, for each region and $E_{\mathrm{T}}^{\mathrm{miss}}$ bin defined in Table 1. The uncertainties shown include both statistical and systematic errors.

WZ/ZZ	$E_{\mathrm{T}}^{\mathrm{miss}}$ [GeV]	50-100	100-150	150-250	250-350	350+
	Template	773.2±31.9	29.3±4.4	2.9±2.1	1.0±0.7	0.3±0.3
	FS	9.4±3.0	11.1±3.6	3.2±1.1	$0.1^{+0.2}_{-0.1}$	$0.1^{+0.2}_{-0.1}$
	Rares	10.4±2.6	14.5±4.0	15.5±5.1	5.0±1.8	2.2±0.9
	Sum	793.0±32.2	54.9±7.0	21.6±5.6	6.0±1.9	2.5±0.9
	Data	793	57	29	2	0
HZ	$E_{\mathrm{T}}^{\mathrm{miss}}$ [GeV]	50-100	100-150	150-250	250+	
	Template	76.7±9.4	2.9±2.4	0.3±0.2	0.1±0.1	
	FS	4.2±1.4	4.0±1.4	4.7±1.6	0.9±0.4	
	Rares	1.1±0.3	0.7±0.2	0.6±0.2	0.3±0.1	
	Sum	82.0±9.5	7.6±2.8	5.6±1.6	1.3±0.4	
	Data	82	9	5	1	

8.2 Results of the edge search

The edge-like search features seven distinct $m_{\ell\ell}$ regions, each of which is divided into two bins using the leptonic likelihood, resulting in fourteen signal regions. In addition two aggregate regions integrating the mass signal regions below and above the Z boson mass have been considered in the non-$\mathrm{t\bar{t}}$ like case. Table 4 summarizes the SM predictions and the observations in these signal regions. A graphical representation of these results is shown in Fig. 5, including the relative contributions of the different backgrounds.

Table 4: Results of the edge-search counting experiment for event yields in the signal regions. The statistical and systematic uncertainties are added in quadrature.

Mass range [GeV]	FS	Template	Rares	Sum	Observed
		$\mathrm{t\bar{t}}$ like			
20-60	$290.9^{+20.7}_{-19.7}$	0.4±0.3	1.4±0.5	$292.7^{+20.7}_{-19.7}$	273
60-86	$180.5^{+15.7}_{-14.7}$	0.9±0.7	8.8±3.4	$190.1^{+16.1}_{-15.1}$	190
96-150	$175.5^{+15.4}_{-14.4}$	1.1±0.9	6.0±2.4	$182.7^{+15.7}_{-14.6}$	192
150-200	$73.3^{+10.4}_{-9.2}$	0.1±0.1	0.4±0.2	$73.9^{+10.4}_{-9.2}$	66
200-300	$46.9^{+8.4}_{-7.3}$	0.1±0.1	0.3±0.1	$47.3^{+8.4}_{-7.3}$	42
300-400	$18.5^{+5.7}_{-4.5}$	0.0±0.0	0.0±0.0	$18.6^{+5.7}_{-4.5}$	11
>400	$4.3^{+3.4}_{-2.1}$	0.0±0.0	0.1±0.0	$4.5^{+3.4}_{-2.1}$	4
		non-$\mathrm{t\bar{t}}$ like			
20-60	$3.3^{+3.2}_{-1.8}$	0.7±0.5	1.4±0.5	$5.3^{+3.3}_{-1.9}$	6
60-86	$3.3^{+3.2}_{-1.8}$	1.6±1.3	6.9±2.7	$11.8^{+4.4}_{-3.5}$	19
96-150	$6.6^{+3.9}_{-2.6}$	1.9±1.5	6.8±2.7	$15.3^{+5.0}_{-4.1}$	28
150-200	$5.5^{+3.7}_{-2.4}$	0.2±0.3	0.7±0.3	$6.4^{+3.7}_{-2.4}$	7
200-300	$3.3^{+3.2}_{-1.8}$	0.2±0.2	0.5±0.2	$3.9^{+3.2}_{-1.8}$	4
300-400	$3.3^{+3.2}_{-1.8}$	0.1±0.1	0.2±0.1	$3.5^{+3.2}_{-1.8}$	0
>400	$1.1^{+2.5}_{-0.9}$	0.1±0.1	0.4±0.2	$1.6^{+2.5}_{-0.9}$	5
		Super signal regions (non-$\mathrm{t\bar{t}}$ like)			
20-86	$6.5^{+3.9}_{-2.6}$	2.3±1.5	8.3±3.2	$17.1^{+5.3}_{-4.4}$	25
>96	$19.6^{+5.8}_{-4.6}$	2.4±1.6	8.5±3.4	$30.6^{+7.0}_{-6.0}$	44

At high mass and in the non-$\mathrm{t\bar{t}}$ like regions the uncertainty on the background prediction is driven by the statistical uncertainty on the number of events in the OF sample. There is agreement between observation and prediction for all signal regions, except for the non-$\mathrm{t\bar{t}}$ like region for masses between 96 and 150 GeV, where a 2.0 standard deviations (local significance) excess is observed.

The dilepton mass distributions and the results of the kinematic fit are shown in Fig. 6. Table 5 presents a summary of the fit results. A signal yield of 61.4 ± 27.9 events is obtained when evaluating the signal hypothesis in the baseline signal region, with an edge located at $144.2^{+3.3}_{-2.2}$ GeV. This is in agreement with the upwards fluctuations in the mass regions between 96 and 150 GeV in the counting experiment. To estimate the p-value of the result, the test statistic $-2\ln Q$, where Q denotes the ratio of the fitted likelihood value for the signal-plus-background hypothesis to the background-only hypothesis, is evaluated on data and compared to the respective quantity on a large sample of background only toy MC. The resulting p-value is interpreted as the one-sided tail probability of a Gaussian distribution and corresponds to

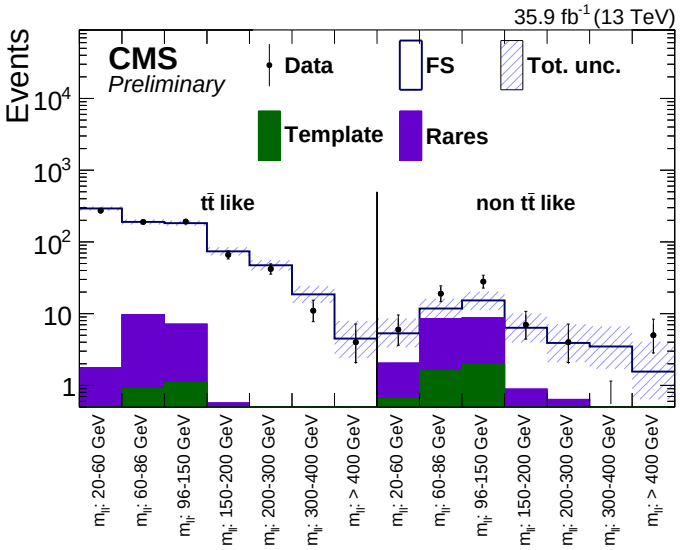

Figure 5: Results of the counting experiment of the edge search. For each signal region, the number of observed events, shown as black data points, is compared to the total background estimate, shown as a blue line with a blue uncertainty band. The non flavor symmetric background component from instrumental $E_{\mathrm{T}}^{\mathrm{miss}}$ is indicated as a green area while the non flavor symmetric background with neutrinos is shown as a violet area.

an excess in the observed number of events compared to the SM background prediction of 2.3(1.5) σ local (global) standard deviations.

Table 5: Results of the unbinned maximum likelihood fit for event yields in the signal region, including the DY and FS background components, along with the fitted signal contribution and edge position. The fitted value for $R_{\mathrm{SF/OF}}$ and the local and global signal significances are also given. The quoted uncertainties account for both statistical and systematic sources.

Drell–Yan	191 ± 19
OF yield	768 ± 24
$R_{\mathrm{SF/OF}}$	1.07 ± 0.03
Signal events	61.4 ± 27.9
$m_{\ell\ell}^{\mathrm{edge}}$	$144.2^{+3.3}_{-2.2}$ GeV
Local significance	2.3 σ
Global significance	1.5 σ

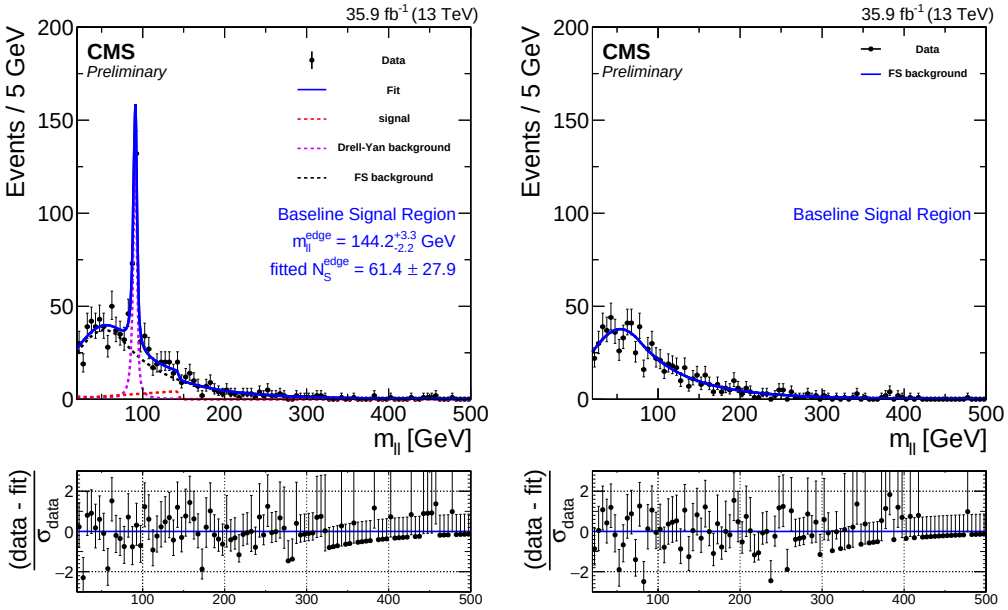

Figure 6: Fit of the dilepton mass distributions to thesignal-plus-background hypothesis in the baseline signal region, projected on the same-flavor (left) and opposite-flavor (right) event samples. The fit shape is shown as a blue, solid line. The individual fit components are indicated by dashed lines. The flavor-symmetric (FS) background is shown with a black dashed line. The Drell–Yan (DY) background is displayed with a purple dashed line. The extracted signal component is displayed with a red dashed line.

9 Interpretation

The results are interpreted in terms of the simplified models defined in Section 4. Upper limits on the cross section multiplied by the branching ratio have been calculated at a 95% confidence level (CL) using the CL_S criterion and an asymptotic formulation [55–58], taking into account the statistical and systematic uncertainties in the signal yields and the background predictions.

9.1 Systematic uncertainty in the signal yield

The systematic uncertainties in the signal yield have been evaluatedcomparing nominal yields, and the ones after making a variation on thesource of the systematic effect. The uncertainty related to the measurement of the integrated luminosity is 2.6%. The uncertainty in the corrections used to account for lepton identification and isolation efficiency differences between data and simulation results in an uncertainty of 5% in the signal acceptance. The uncertainty in the b tagging efficiency and mistag probability are 0–5% depending on the signal model and masses probed. A further systematic uncertainty of 4% is considered on the scale factors correcting for the differences between fast and GEANT4 simulations for leptons. Dilepton trigger efficiencies ranging between 91% and 96%, and depending on the lepton flavor, are measured in data and applied as an overall scale factor to the signal simulation with a systematic uncertainty of 3%. The uncertainty in the jet energy scale varies between 0% and 5% depending on the signal kinematics. The uncertainty associated with the modeling of initial-state radiation (ISR) is 0–2.5%. Determining the signal acceptance in a high pileup and low pileup regime separately, yields an uncertainty of 1–2%. To account for uncertainties in $E_{\mathrm{T}}^{\mathrm{miss}}$ in fast simulation, the evaluation of the signal yield is repeated using generator $E_{\mathrm{T}}^{\mathrm{miss}}$. The average of both yields is used for the signal yields and the difference between this value and the yield using standard $E_{\mathrm{T}}^{\mathrm{miss}}$ is used as an uncertainty, ranging from 0–4%. Finally the statistical uncertainty on the number of simulated events is also considered and found to be in the range 1–15%, depending on the signal region and mass point. These uncertainties are summarized in Table 6.

Table 6: Systematic uncertainties taken into account for the signal yields and their typical values.

Source of uncertainty	Uncertainty (%)
Luminosity	2.6
Pileup	1–2
b tag modeling	0–5
Lepton reconstruction and isolation	5
Fast simulation scale factors	4
Fast simulation MET uncertainty	0–4
Trigger modeling	3
Jet energy scale	0–5
ISR modeling	0–2.5
Q^2 scale	1–3
Statistical uncertainty	1–15
Total uncertainty	9–18

9.2 Interpretations using simplified models

The gluino GMSB model leads to a signature containing at least 6 jets in the final state when one of the Z bosons decays leptonically and the other decays hadronically. Therefore most of the sensitivity of the on-Z search is provided by the high jet multiplicity signal regions defined within the SRC category. All of the strong on-Z regions are considered, however, to set limits in this model. The expected and observed limits are presented in Fig. 7. We are able to probe gluino masses up to 1500–1770 GeV depending on the mass of $\tilde{\chi}_1^0$. This represents an improvement of around 500 GeV compared to the previously published CMS result [13].

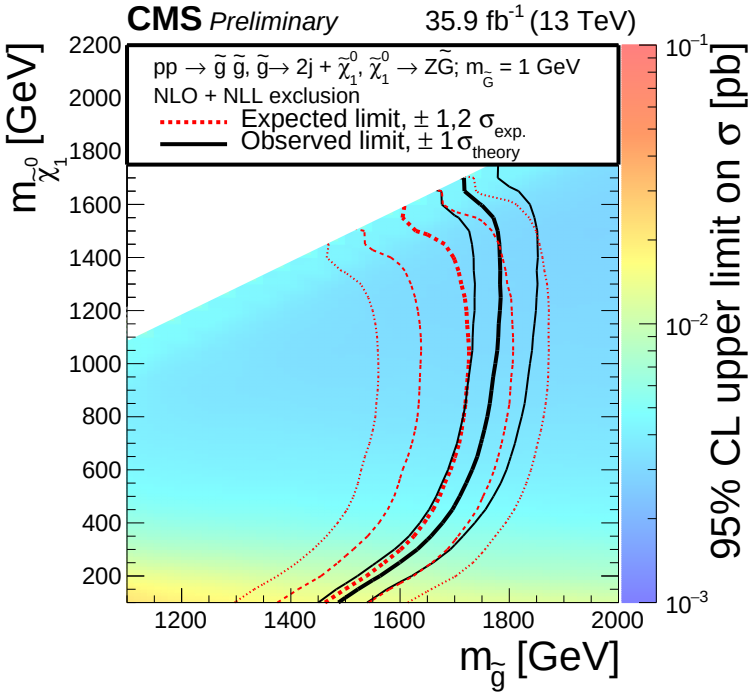

Figure 7: Cross section upper limits and exclusions contours at 95% CL obtained from the results of the on-Z search interpreted in the gluino GMSB model. The region to the left of the red dotted (black solid) line shows the masses which are excluded by the expected (observed) limit.

The on-Z search for electroweak production is interpreted using the model descried in Sec. 4. For the model of $\tilde{\chi}_1^{\pm}$-$\tilde{\chi}_2^0$ production decaying to WZ, the VZ signal regions primarily contribute. Figure 8 shows the cross section upper limits and the exclusion lines at 95% CL as a function of the $\tilde{\chi}_1^{\pm}$ and $\tilde{\chi}_1^0$ masses. The analysis is sensitive for $\tilde{\chi}_1^{\pm}$ masses between approximately 160 and 610 GeV, depending on the mass of $\tilde{\chi}_1^0$.

The edge search is interpreted using the slepton-edge model, combining the seven invariant mass bins and the two likelihood regions. Figure 9 shows the exclusion contour as a function of the bottom squark mass and the second neutralino mass. We exclude bottom squark masses up to 1200 GeV. A decrease of the sensitivity is observed for those models where the neutralino mass is in the range $\sim$ 200–250 GeV. The $m_{\ell\ell}$ distribution for these kind of models has an edge in the range $\sim$ 100–150 GeV, and most of the signal events fall into the signal regions with the highest background prediction or in the invariant mass region close to the Z boson mass which is vetoed for this part of the analysis. The observed limit in this regime is weaker than the expected one due to the 2.0 σ deviation in the non-$t\bar{t}$ like, 96-150 GeV mass bin. For high $\tilde{\chi}_2^0$

masses, the majority of signal events fall into the highest mass bins, which are nearly background free. This results in an increased sensitivity for these mass points. In the highest non-$t\bar{t}$ like mass bin, 5 events are observed and 1.5 expected, yielding a weaker observed limit for these mass points. The 300-400 GeV non-$t\bar{t}$ like mass bin contains 0 observed events compared to an expectation of 3.5 and causes the stronger observed limit on the $\tilde{\chi}_2^0$ mass of about 500 GeV.

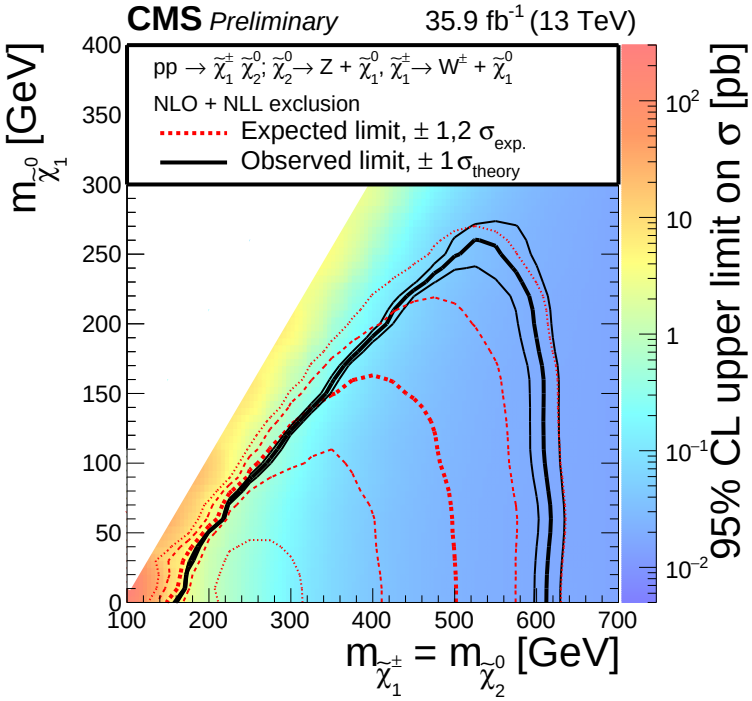

Figure 8: Cross section upper limits and exclusions contours at 95% CL obtained from the results of the on-Z search interpreted in the electroweak WZ model. The region to the left of the red dotted (black solid) line shows the masses which are excluded by the expected (observed) limit.

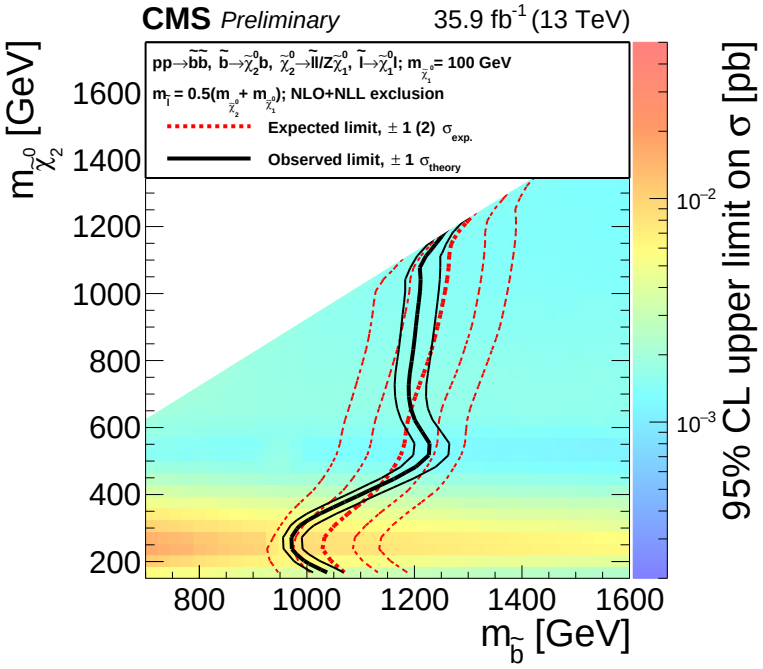

Figure 9: Cross section upper limits and exclusion contours at 95% CL obtained from the results of the edge search interpreted in the slepton-edge model. The region to the left of the red dotted (black solid) line shows the masses which are excluded by the expected (observed) limit.

10 Summary

A search for physics beyond the standard model has been presented in the opposite-sign, same-flavor lepton; jets; and $E_{\mathrm{T}}^{\mathrm{miss}}$ final state using a data sample of pp collisions collected with the CMS detector in 2016 at a center-of-mass energy of 13 TeV, corresponding to an integrated luminosity of 35.9 fb^{-1}. Searches are performed for signals that either produce a kinematic edge in the dilepton invariant mass, or use dilepton systems whose invariant mass is compatible with the decay of a Z boson. Comparing the observation to estimates for SM backgrounds obtained from data control samples, and no statistically significant evidence for a signal has been observed.

The search for strongly produced new physics containing an on-shell Z boson is interpreted in a model of gauge-mediated supersymmetry breaking, where the Z bosons are produced in decay chains initiated through gluino pair production. Gluino masses below 1500–1770 GeV have been excluded, depending on the neutralino mass, extending the previous exclusion limits derived from the previous CMS publication by almost 500 GeV.

The electroweak on-Z search has been interpreted in a simplified model of chargino-neutralino production where the neutralino decays to a Z boson and the LSP, and the chargino decays to a W boson and the LSP. In this model, we probe chargino masses in the range 160–610 GeV.

The searchfor a kinematic edge in the $m_{\ell\ell}$ distribution is interpreted in a simplified model based on bottom squark pair production, where dilepton mass edges are produced in decay chains containing the two lightest neutralinos and a slepton, where the branching ratios have been fixed to produce the desired topology. Bottom squark masses below 980 to 1200 GeV have been excluded, depending on the $\tilde{\chi}_2^0$ mass. These limits extend previous exclusion limits by 400–600 GeV depending also on the $\tilde{\chi}_2^0$ mass.

References

[1] P. Ramond, "Dual theory for free fermions", *Phys. Rev. D* **3** (1971) 2415, doi:10.1103/PhysRevD.3.2415.

[2] Y. A. Golfand and E. P. Likhtman, "Extension of the algebra of Poincaré group generators and violation of P invariance", *JETP Lett.* **13** (1971) 323.

[3] A. Neveu and J. H. Schwarz, "Factorizable dual model of pions", *Nucl. Phys. B* **31** (1971) 86, doi:10.1016/0550-3213(71)90448-2.

[4] D. V. Volkov and V. P. Akulov, "Possible universal neutrino interaction", *JETP Lett.* **16** (1972) 438.

[5] J. Wess and B. Zumino, "A Lagrangian model invariant under supergauge transformations", *Phys. Lett. B* **49** (1974) 52, doi:10.1016/0370-2693(74)90578-4.

[6] J. Wess and B. Zumino, "Supergauge transformations in four dimensions", *Nucl. Phys. B* **70** (1974) 39, doi:10.1016/0550-3213(74)90355-1.

[7] P. Fayet, "Supergauge invariant extension of the Higgs mechanism and a model for the electron and its neutrino", *Nucl. Phys. B* **90** (1975) 104, doi:10.1016/0550-3213(75)90636-7.

[8] H. P. Nilles, "Supersymmetry, supergravity and particle physics", *Phys. Rep.* **110** (1984) 1, doi:10.1016/0370-1573(84)90008-5.

[9] G. R. Farrar and P. Fayet, "Phenomenology of the Production, Decay, and Detection of New Hadronic States Associated with Supersymmetry", *Phys. Lett. B* **76** (1978) 575, doi:10.1016/0370-2693(78)90858-4.

[10] G. Buras, Ellis and Nanopoulos, "Aspects of the grand unification of strong, weak and electromagnetic interactions", *Nuclear Physics B* **135** (1978), no. 1, 66, doi:10.1016/0550-3213(78)90214-6.

[11] Haber and Kane, "The search for supersymmetry: Probing physics beyond the standard model", *Physics Reports* **117** (1985), no. 2, 75, doi:10.1016/0370-1573(85)90051-1.

[12] CMS Collaboration, "Search for Physics Beyond the Standard Model in Events with Two Leptons, Jets, and Missing Transverse Momentum in pp Collisions at $\sqrt{s} = 8$ TeV", *JHEP* **04** (2015) 124, doi:10.1007/JHEP04(2015)124, arXiv:1502.06031.

[13] CMS Collaboration, "Search for new physics in final states with two opposite-sign, same-flavor leptons, jets, and missing transverse momentum in pp collisions at $\sqrt{s}$ = 13 TeV", *JHEP* **12** (2016) 013, doi:10.1007/JHEP12(2016)013, arXiv:1607.00915.

[14] CMS Collaboration, "Search for new physics in events with opposite-sign leptons, jets, and missing transverse energy in pp collisions at $\sqrt{s} = 7$ TeV", *Physics Letters B* **718** (2013), no. 3, 815, doi:10.1016/j.physletb.2012.11.036, arXiv:1206.3949.

[15] CMS Collaboration, "Search for physics beyond the standard model in opposite-sign dilepton events in pp collisions at $\sqrt{s} = 7$ TeV", *Journal of High Energy Physics* **2011** (2011), no. 6, 26, doi:10.1007/JHEP06(2011)026, arXiv:1103.1348.

[16] CMS Collaboration, "Searches for electroweak production of charginos, neutralinos, and sleptons decaying to leptons and W, Z, and Higgs bosons in pp collisions at 8 TeV", *The European Physical Journal C* **74** (2014), no. 9, 1, doi:10.1140/epjc/s10052-014-3036-7, arXiv:1405.7570.

[17] CMS Collaboration, "Searches for electroweak neutralino and chargino production in channels with Higgs, Z, and W bosons in pp collisions at 8 TeV", *Phys. Rev. D* **90** (Nov, 2014) 092007, doi:10.1103/PhysRevD.90.092007, arXiv:1409.3168.

[18] ATLAS Collaboration, "Search for supersymmetry in events containing a same-flavour opposite-sign dilepton pair, jets, and large missing transverse momentum in $\sqrt{s} = 8$ TeV pp collisions with the ATLAS detector", *Eur. Phys. J. C* **75** (2015) 318, doi:10.1140/epjc/s10052-015-3661-9, 10.1140/epjc/s10052-015-3518-2, arXiv:1503.03290. [Erratum: *Eur. Phys. J. C* **75** (2015) 463].

[19] ATLAS Collaboration, "Search for the electroweak production of supersymmetric particles in $\sqrt{s} = 8$ TeV pp collisions with the ATLAS detector", *Phys. Rev. D* **93** (Mar, 2016) 052002, doi:10.1103/PhysRevD.93.052002, arXiv:1509.07152.

[20] ATLAS Collaboration, "Search for new phenomena in events containing a same-flavour opposite-sign dilepton pair, jets, and large missing transverse momentum in $\sqrt{s} = 13$ TeV pp collisions with the ATLAS detector", arXiv:1611.05791.

[21] I. Hinchliffe et al., "Precision SUSY measurements at CERN LHC", *Phys. Rev. D* **55** (1997) 5520, doi:10.1103/PhysRevD.55.5520, arXiv:hep-ph/9610544.

[22] CMS Collaboration, "The CMS experiment at the CERN LHC", *JINST* **3** (2008) S08004, doi:10.1088/1748-0221/3/08/S08004.

[23] CMS Collaboration, "Particle-Flow Event Reconstruction in CMS and Performance for Jets, Taus, and MET", Technical Report CMS-PAS-PFT-09-001, CERN, 2009. Geneva, Apr, 2009.

[24] CMS Collaboration, "Commissioning of the Particle-flow Event Reconstruction with the first LHC collisions recorded in the CMS detector", Technical Report CMS-PAS-PFT-10-001, 2010.

[25] CMS Collaboration, "Performance of electron reconstruction and selection with the CMS detector in proton-proton collisions at $\sqrt{s} = 8$ TeV", *JINST* **10** (2015) P06005, doi:10.1088/1748-0221/10/06/P06005, arXiv:1502.02701.

[26] CMS Collaboration, "Performance of photon reconstruction and identification with the CMS detector in proton-proton collisions at $\sqrt{\mathrm{s}} = 8$ TeV", *Journal of Instrumentation* **10** (2015), no. 08, P08010.

[27] M. Cacciari, G. P. Salam, and G. Soyez, "The anti-k_t jet clustering algorithm", *JHEP* **04** (2008) 063, doi:10.1088/1126-6708/2008/04/063, arXiv:0802.1189.

[28] M. Cacciari, G. P. Salam, and G. Soyez, "FastJet user manual", *Eur. Phys. J. C* **72** (2012) 1896, doi:10.1140/epjc/s10052-012-1896-2, arXiv:1111.6097.

[29] M. Cacciari and G. P. Salam, "Dispelling the N^3 myth for the k_t jet-finder", *Phys. Lett. B* **641** (2006) 57, doi:10.1016/j.physletb.2006.08.037, arXiv:hep-ph/0512210.

[30] CMS Collaboration, "Determination of Jet Energy Calibration and Transverse Momentum Resolution in CMS", *JINST* **6** (2011) P11002, doi:10.1088/1748-0221/6/11/P11002, arXiv:1107.4277.

[31] M. Cacciari and G. P. Salam, "Pileup subtraction using jet areas", *Phys. Lett. B* **659** (2008) 119, doi:10.1016/j.physletb.2007.09.077, arXiv:0707.1378.

[32] CMS Collaboration, "Identification of b quark jets at the CMS Experiment in the LHC Run 2", Technical Report CMS-PAS-BTV-15-001, 2016.

[33] J. Alwall et al., "The automated computation of tree-level and next-to-leading order differential cross sections, and their matching to parton shower simulations", *JHEP* **07** (2014) 079, doi:10.1007/JHEP07(2014)079, arXiv:1405.0301.

[34] S. Alioli, P. Nason, C. Oleari, and E. Re, "NLO single-top production matched with shower in POWHEG: s- and t-channel contributions", *JHEP* **11** (2010) 111, doi:10.1007/JHEP02(2010)011, 10.1088/1126-6708/2009/09/111, arXiv:0907.4076v2.

[35] E. Re, "Single-top Wt-channel production matched with parton showers using the POWHEG method", *Eur. Phys. J. C* **71** (2011) 1547, doi:10.1140/epjc/s10052-011-1547-z, arXiv:1009.2450.

[36] R. Gavin, Y. Li, F. Petriello, and S. Quackenbush, "FEWZ 2.0: A code for hadronic Z production at next-to-next-to-leading order", *Comput. Phys. Commun.* **182** (2011) 2388–2403, doi:10.1016/j.cpc.2011.06.008, arXiv:1011.3540.

[37] R. Gavin, Y. Li, F. Petriello, and S. Quackenbush, "W Physics at the LHC with FEWZ 2.1", *Comput. Phys. Commun.* **184** (2013) 208–214, doi:10.1016/j.cpc.2012.09.005, arXiv:1201.5896.

[38] M. Czakon and A. Mitov, "Top++: A Program for the Calculation of the Top-Pair Cross-Section at Hadron Colliders", *Comput. Phys. Commun.* **185** (2014) 2930, doi:10.1016/j.cpc.2014.06.021, arXiv:1112.5675.

[39] C. Borschensky et al., "Squark and gluino production cross sections in pp collisions at $\sqrt{s}$ = 13, 14, 33 and 100 TeV", *Eur. Phys. J. C* **74** (2014), no. 12, 3174, doi:10.1140/epjc/s10052-014-3174-y, arXiv:1407.5066.

[40] B. Fuks, M. Klasen, D. R. Lamprea, and M. Rothering, "Gaugino production in proton-proton collisions at a center-of-mass energy of 8 TeV", *JHEP* **10** (2012) 081, doi:10.1007/JHEP10(2012)081, arXiv:1207.2159.

[41] B. Fuks, M. Klasen, D. R. Lamprea, and M. Rothering, "Precision predictions for electroweak superpartner production at hadron colliders with RESUMMINO", *Eur. Phys. J. C* **73** (2013) 2480, doi:10.1140/epjc/s10052-013-2480-0, arXiv:1304.0790.

[42] J. Alwall et al., "The automated computation of tree-level and next-to-leading order differential cross sections, and their matching to parton shower simulations", *JHEP* **07** (2014) 079, doi:10.1007/JHEP07(2014)079, arXiv:1405.0301.

[43] S. Frixione, P. Nason, and C. Oleari, "Matching NLO QCD computations with Parton Shower simulations: the POWHEG method", *JHEP* **11** (2007) 070, doi:10.1088/1126-6708/2007/11/070, arXiv:0709.2092.

[44] T. Sjostrand, S. Mrenna, and P. Z. Skands, "A Brief Introduction to PYTHIA 8.1", *Comput. Phys. Commun.* **178** (2008) 852–867, doi:10.1016/j.cpc.2008.01.036, arXiv:0710.3820.

[45] NNPDF Collaboration, "Parton distributions for the LHC Run II", *JHEP* **04** (2015) 040, doi:10.1007/JHEP04(2015)040, arXiv:1410.8849.

[46] GEANT4 Collaboration, "GEANT4 — a simulation toolkit", *Nucl. Instrum. Meth. A* **506** (2003) 250, doi:10.1016/S0168-9002(03)01368-8.

[47] S. Abdullin et al., "The fast simulation of the CMS detector at LHC", *J. Phys. Conf. Ser.* **331** (2011) 032049, doi:10.1088/1742-6596/331/3/032049.

[48] K. T. Matchev and S. D. Thomas, "Higgs and Z boson signatures of supersymmetry", *Phys. Rev. D* **62** (2000) 077702, doi:10.1103/PhysRevD.62.077702, arXiv:hep-ph/9908482.

[49] P. Meade, M. Reece, and D. Shih, "Prompt decays of general neutralino NLSPs at the Tevatron", *JHEP* **05** (2010) 105, doi:10.1007/JHEP05(2010)105, arXiv:0911.4130.

[50] J. T. Ruderman and D. Shih, "General neutralino NLSPs at the early LHC", *JHEP* **08** (2012) 159, doi:10.1007/JHEP08(2012)159, arXiv:1103.6083.

[51] C. G. Lester and D. J. Summers, "Measuring masses of semiinvisibly decaying particles pair produced at hadron colliders", *Phys. Lett. B* **463** (1999) 99, doi:10.1016/S0370-2693(99)00945-4, arXiv:hep-ph/9906349.

[52] A. Barr, C. Lester, and P. Stephens, "A variable for measuring masses at hadron colliders when missing energy is expected; M_{T2} : the truth behind the glamour", *J. Phys. G* **29** (2003) 2343, doi:10.1088/0954-3899/29/10/304, arXiv:hep-ph/0304226.

[53] M. J. Oreglia, "A study of the reactions $\psi' \to \gamma\gamma\psi$". PhD thesis, Stanford University, 1980. SLAC Report SLAC-R-236, see Appendix D.

[54] Olive et al., "Review of Particle Physics", *Chin. Phys. C* **38** (2014) 090001, doi:10.1088/1674-1137/38/9/090001.

[55] T. Junk, "Confidence level computation for combining searches with small statistics", *Nucl. Instrum. Meth. A* **434** (1999) 435, doi:10.1016/S0168-9002(99)00498-2, arXiv:hep-ex/9902006.

[56] A. L. Read, "Presentation of search results: the CL_s technique", *J. Phys. G* **28** (2002) 2693, doi:10.1088/0954-3899/28/10/313.

[57] ATLAS and CMS Collaborations, "Procedure for the LHC Higgs boson search combination in summer 2011", Technical Report ATL-PHYS-PUB-2011-011, CMS-NOTE-2011-005, CERN, 2011.

[58] G. Cowan, K. Cranmer, E. Gross, and O. Vitells, "Asymptotic formulae for likelihood-based tests of new physics", *Eur. Phys. J. C* **71** (2011) 1554, doi:10.1140/epjc/s10052-011-1554-0, 10.1140/epjc/s10052-013-2501-z, arXiv:1007.1727. [Erratum: *Eur. Phys. J. C* **73** (2013) 2501].

[59] CMS Collaboration, "Simplified likelihood for the re-interpretation of public CMS results", Technical Report CMS-NOTE-2017-001. CERN-CMS-NOTE-2017-001, CERN, Geneva, Jan, 2017.

A Correlation and covariance matrices for the background predictions

In order to ease the interpretation of the results in other models, we provide the covariance and correlation matrices for the background predictions in the different signal regions. Figure 10 shows a graphical representation of the covariance (left) and correlation (right) matrices for the on-Z strong signal regions. Figure 11 shows the same matrices for the on-Z electroweak signal regions, and Fig. 12 the corresponding matrices for the edge strong signal regions. This information can be used to construct a simplified likelihood for models of new physics, as described in Ref. [59].

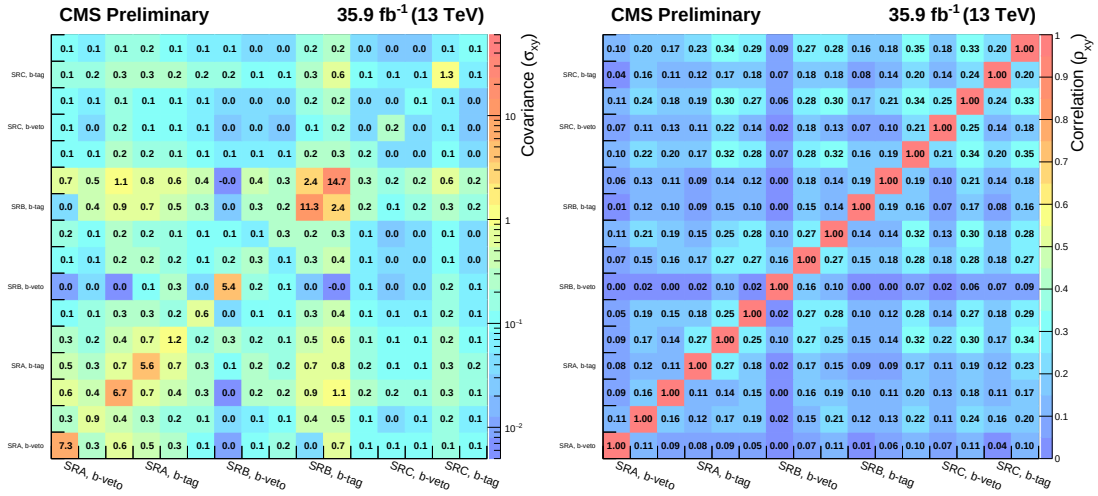

Figure 10: The covariance (left) and correlation (right) matrices for the background predictions in the on-Z strong signal regions. Within each signal region, the individual $E_{\mathrm{T}}^{\mathrm{miss}}$ bins are shown in increasing order starting from 100 GeV.

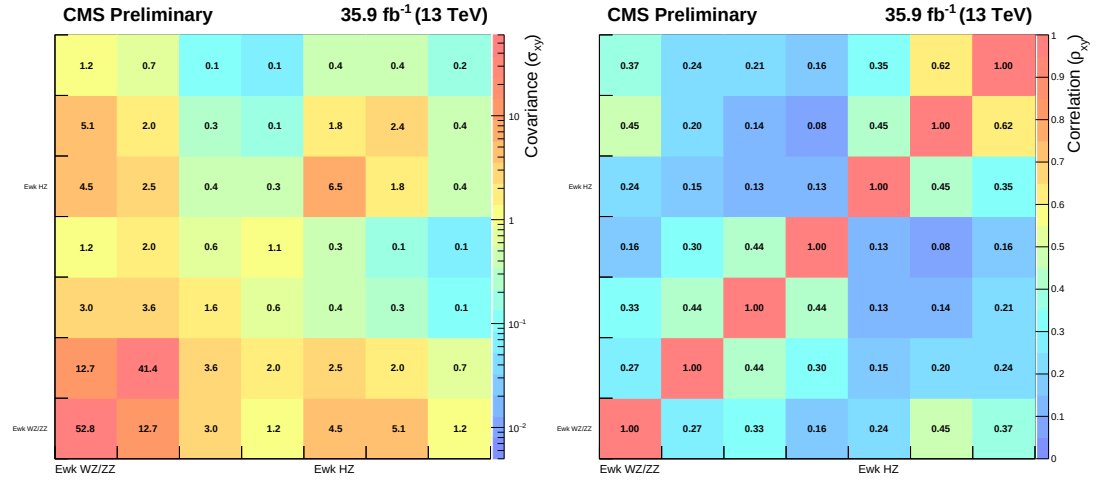

Figure 11: The covariance (left) and correlation (right) matrices for the background predictions in the on-Z electroweak signal regions. Within each signal region, the individual $E_{\mathrm{T}}^{\mathrm{miss}}$ bins are shown in increasing order starting from 100 GeV.

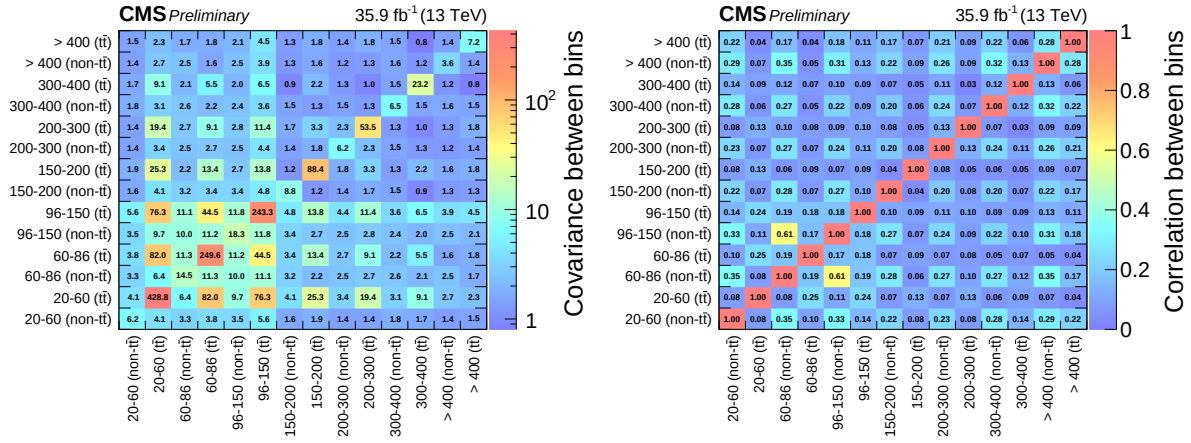

Figure 12: The covariance (left) and correlation (right) matrices for the background predictions in the edge strong signal regions.